# Local and intermediate-range structure of amorphous $MoS_3$: Model calculation study

F. Z. Chien* and S. C. Moss
*Physics Department, University of Houston, University Park, Houston, Texas 77004*

K. S. Liang and R. R. Chianelli
*Corporate Research Science Laboratories, Exxon Research and Engineering Company, P.O. Box 45, Linden, New Jersey 07036*
(Received 20 October 1983)

The amorphous phase of $MoS_3$, which has no crystalline counterpart, is prepared through the thermal decomposition of ammonium thiomolybdate. The structure of this amorphous phase has been analyzed through a combination of x-ray diffraction and computer calculation of model structures. Both the x-ray diffraction pattern and its Fourier transform, the pair distribution function, were modeled. In $r$ space there were four prominent distances whose positions and relative contributions required fitting while in $k$ space there was a prominent well-defined peak at $\sim 1$ Å$^{-1}$ together with diffuse oscillations out to $\sim 15$–$16$ Å$^{-1}$. Relevant spectroscopic and chemical data were used to rationalize a consistent structure. A basic chainlike arrangement of dimerized Mo atoms separated by triangularly coordinated S atoms with disulfur bonds, provided the starting point. The final structure consisted of pairs of (coupled) chains with significant deviations or bendings from parallel alignment. These paired flat chains could then be stacked as they would naturally be in the material to produce the requisite planar correlations for the 1-Å$^{-1}$ peak in $k$ space. The final overall fit in both $k$ and $r$ space was considered good.

## I. INTRODUCTION

The structures of amorphous materials have been widely studied and are known, in most cases, to have some type of short-range order among nearest-neighbor atoms.[1] Many of the materials studied demonstrate structural correlation well beyond the nearest-neighbor distances as well. These intermediate-range structural correlations (intermediate between nearest neighbors and the long-range order of crystals) are often observed as prominent diffraction peaks in the low-$k$ region where $k = 4\pi \sin\theta/\lambda$ and $2\theta$ is the angle between the incident and scattered rays. In our view, the characteristics of the intermediate structure make the amorphous phase distinctively different from the crystalline one and are essential for understanding the properties of amorphous materials. It is the purpose of this study to investigate this extended structure in a novel material, amorphous ($a$-) $MoS_3$.

Experimentally, the elucidation of the intermediate-range structure of amorphous materials is difficult and constitutes a challenge to our visualization of these materials. First of all, there is a lack of experimental methods. Although many techniques can be applied to probe the local structure in amorphous materials, including EXAFS (extended x-ray-absorption fine structure), NMR, XPS (x-ray photoelectron spectroscopy), Raman and ir vibrational spectroscopies, Mössbauer spectroscopy, and so forth, the most direct probe of the intermediate-range structure remains the scattering methods with x rays, neutrons, or electrons. An attendant complication arises in the interpretation of the diffuse scattering intensity from amorphous bodies, however, which is often not straightforward. In this regard, it is understandable that, although many structural models of amorphous materials have been constructed, the connections between these models and the "true" structure remain mostly to be tested.[2] We pursue this course with $a$-$MoS_3$ using a ball-and-stick model building technique to interpret the diffraction data in both $r$ space and $k$ space. The results prove to be both unusual and nonintuitive and confirm our belief that $r$ space and $k$ space fitting provide important complementary information.

Amorphous $MoS_3$ is an interesting material which, along with $MoSe_3$, $WS_3$, and $WSe_3$, can be prepared only in the amorphous form while the analog crystalline trichalcogenides of the neighboring groups IV$B$ (Ti, Zr, Hf) and V$B$ (Nb, Ta) are known to have chainlike structures.[3] More recently, $a$-$MoS_3$ was found to have interesting electrochemical properties.[4] It can react readily and reversibly with three lithium atoms per $MoS_3$ unit at room temperature which is a substantially better capacity than shown by, say, crystalline $ZrS_3$ which reacts with only one lithium per $ZrS_3$ unit. It would therefore be additionally interesting to investigate the extent of similarity between amorphous and crystalline trichalcogenides from a structural point of view.

In this work, computer calculations on model structures of $a$-$MoS_3$ are compared with x-ray diffraction data presented in both $k$ space and $r$ space. The results show that $a$-$MoS_3$ possesses a rather unique structure which may be termed a ribbonlike arrangement of paired dimerized chains with appropriate intrachain and interchain connections to conform to the chemical, spectroscopic, and structural data.

 

## II. EXPERIMENT

### A. Sample preparation

Samples of $a$-$MoS_3$ were prepared by thermal decomposition of the ammonium tetrathio compound $(NH_4)_2MoS_4$ at 200 °C under flowing dry $N_2$ conditions through a well-established reaction:[4]

$$(NH_4)_2MoS_4 \xrightarrow[N_2]{\approx 200\,^\circ C} a\text{-}MoS_3 \xrightarrow[H_2S/H_2]{\geq 400\,^\circ C} \text{pc-}MoS_2 .$$

A typical thermogravimetric curve of this reaction is shown in Fig. 1. The curve shows a plateau region at a temperature near 300 °C, which corresponds to a weight loss of 26.24% from $(NH_4)_2MoS_4$. This value is close to the theoretical weight loss of 26.16% for the formation of $MoS_3$. It is interesting to note that the compositions of the amorphous compounds typically obtained by this means are very close to $MX_3$ stoichiometry. Continuing the process in Fig. 1 to higher temperature in the presence of an $H_2S/H_2$ gas mixture leads eventually to the poorly crystallized (pc-) state of $MoS_2$.

### B. Data collection and refinement

The x-ray experiment was performed at the Stanford Synchrotron Radiation Laboratory on beam line I-5 where the radiation is obtained from a bending magnet. The ring was operated at 3.0 GeV and 50 mA. The high intensity, the almost completely polarized beam, and the free selection of x-ray wavelength provided by the synchrotron is clearly to our advantage in comparison with a conventional laboratory Cu or Mo source for the $MoS_3$ study.

The measurements employed 19-keV x-ray photons using the Si(111) monochromator of beam line I-5. This wavelength (0.652 Å) is below the molybdenum absorption edge to prevent fluorescence but is short enough to obtain the important high-$k$ data. A helium gas flow was set up through the path of the beam and sample chamber to eliminate air scattering. The experiment was carried out to 17.5 $Å^{-1}$. The data analysis will deal with the data below 15.0 $Å^{-1}$, because the high-angle part of the diffraction pattern is often difficult to analyze properly due to uncertainties in the real and imaginary dispersion contributions to the scattering factors.[5]

The measured intensity ($I_m$) was corrected for background ($B$) and Compton scattering [compton-modified (CM)] and then normalized in electron units per unit of composition (uc) to yield the scaled coherently scattered intensity $I'_{eu}/N_{uc}$:

$$I'_{eu}/N_{uc} = n(I_m - B) - [I(\mathrm{CM})]_{uc} ,$$

where $n$ is a normalization constant. Corrections due to absorption and multiple scattering were neglected because of the high absorption coefficient of the sample and the use of the usual symmetrical reflection geometry. A polarization correction was not needed for the near 100% polarized synchrotron radiation.

The Compton-modified intensity in electron units per unit of composition was calculated by using $[I(\mathrm{CM})]_{uc} = R \sum Y(k)$, where

$$R = [\lambda/(\lambda + 0.048\,52 \sin^2\theta)]^3 ,$$

the Breit-Dirac recoil factor,[6] and $Y(k)$ are the tabulated values given in Ref. 7. The normalization constant $n$ is obtained by matching the measured total intensity with

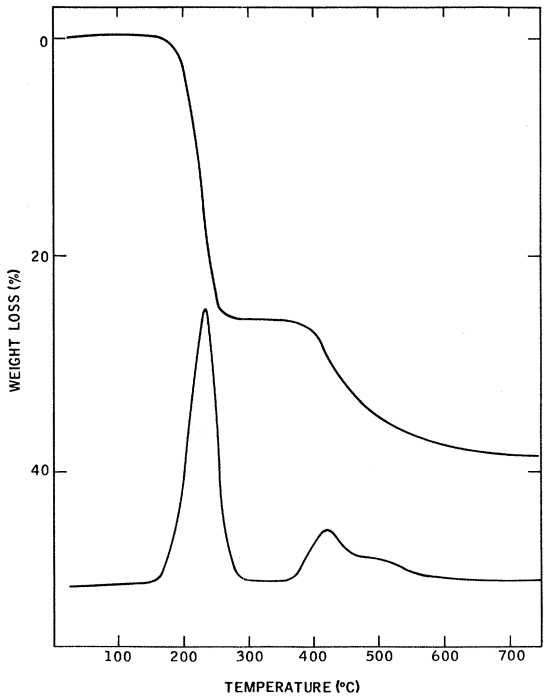


FIG. 1. Thermogravimetric decomposition of $(NH_4)_2MoS_4$; top, thermogram; bottom, differential thermogram. (From Ref. 4.) The first peak in the differential cruve is associated with $a$-$MoS_3$. The second set of peaks are due to the transformation to pc-$MoS_2$.

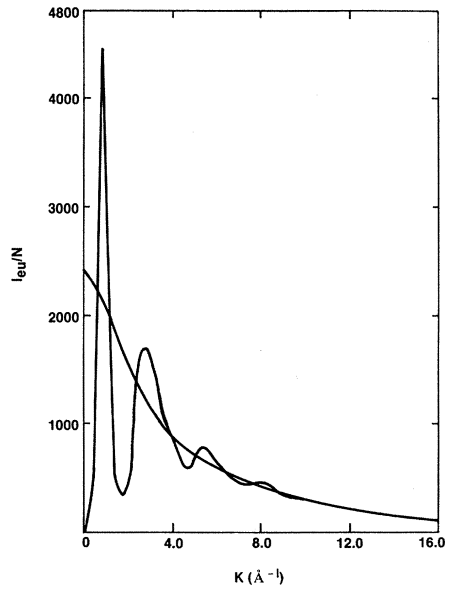


FIG. 2. The normalized intensities of $a$-$MoS_3$, $k=0$ to 16 $Å^{-1}$. Oscillations beyond $k \cong 10.0$ $Å^{-1}$ exist in the data but are not observable on this scale.

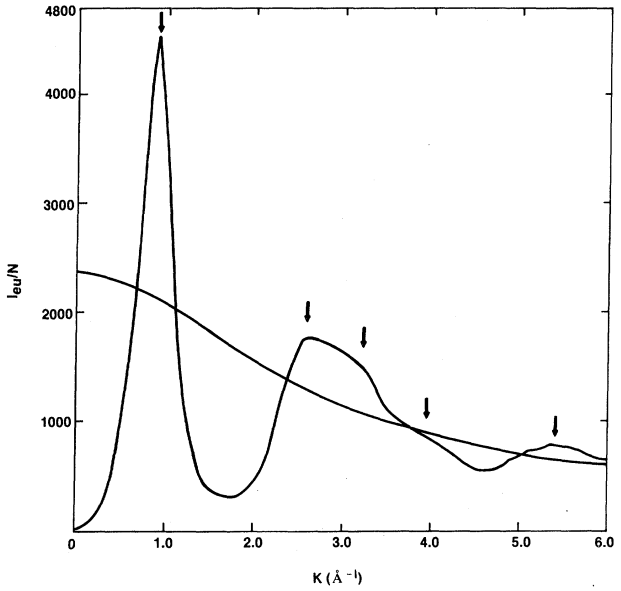


FIG. 3. The normalized intensities of $a$-$MoS_3$, $k=0$ to 6 Å$^{-1}$. The arrows indicate prominent diffuse peaks that will require consideration in the fitting procedure.

the calculated total independent intensity in the high-$k$ region, where the oscillation of the total intensity about the independent scattering curve is small. The total independent scattering curve was calculated using

$$I_t=\sum_{\text{uc}} f_i^2+[I(\text{CM})]_{\text{uc}} .$$

The corrected and scaled intensity of $a$-$MoS_3$ is shown in Fig. 2 and in Fig. 3 for an expanded $k$ scale. The prominent features are evident as indicated by arrows.

## III. DIFFRACTION THEORY

### A. General theory

The process of diffraction is such that the diffracted waves represent the complex transform of the real-space distribution of scattering centers. The x-ray intensity $I_{\text{eu}}$ in electron units is given by[6]

$$I_{\text{eu}}=\sum_m\sum_n f_m f_n \exp[(2\pi i/\lambda)(\vec{S}-\vec{S}_0)\cdot\vec{r}_{mn}] , \tag{1}$$

where $f_m$ is the scattering factor of atom $m$, $\vec{S}$ is the scattering vector of diffracted beam, $\vec{S}_0$ is the scattering vector of incident beam, and $\vec{r}_{mn}=\vec{r}_m-\vec{r}_n$, $\vec{r}_m$ is the position vector of atom $m$.

We consider our sample to be any form of matter in which there is a random orientation of scattering units. This includes gases, liquids, amorphous solids, and small crystalline powders. The average unmodified intensity from an array of atoms which takes all orientations in space is then given by the familiar Debye scattering equation:[6]

$$I_{\text{eu}}=\sum_m\sum_n f_m f_n \frac{\sin(kr_{mn})}{kr_{mn}} , \tag{2}$$

where $k=4\pi\sin\theta/\lambda$ and $2\theta$ is the scattering angle between $\vec{S}$ and $\vec{S}_0$.

For scattering from a real amorphous sample, a general treatment is usually applied by introducing a density function $\rho_m(\vec{r}_{nm})$, such that $\rho_m(\vec{r}_{nm})dV_n$ is the number of atom centers in volume element $dV_n$ at the position $\vec{r}_{nm}$ relative to atom $m$, and by neglecting the small-angle-intensity contribution to give the usual amorphous scattering expression. This neglects both voids in the sample and the shape transform of the entire sample.

If only one kind of atom is present, then spherical averaging allows the expression to be reduced to the usual form[6] as

$$i(k)=\frac{I'_{\text{eu}}/N-f^2}{f^2}$$

$$=\int_0^\infty[\rho(r)-\rho_a]\frac{\sin(kr)}{kr}4\pi r^2\,dr \tag{3}$$

or

$$ki(k)=4\pi\int_0^\infty[\rho(r)-\rho_a]\sin(kr)r\,dr \tag{4}$$

where $ki(k)$ is the partially reduced intensity, usually referred to as the interference function; $\rho(r)=\rho_m(\vec{r}_{nm})$, the average is over all $\rho_m(\vec{r})$ within the sample that are a distance $r$ from an origin atom at $n$ ($\rho_a$ is the average density); and $I'_{\text{eu}}/N$ is the intensity per atom with the small-angle term omitted.

### B. Method of pair function

For a system with more than one kind of atom, an exact method that leads to the pair-distribution solution has been developed by Finbak and recorded by Warren.[6] The pair functions are given by

$$P_{ij}(r)=Q_{ij}(r-r_{ij})-Q_{ij}(r+r_{ij}) \tag{5}$$

and

$$Q_{ij}(x)=\tfrac{1}{2}\int_0^{k_m}\frac{f_i f_j}{g^2(k)}e^{-\alpha^2k^2}\cos(kr)dk . \tag{6}$$

$Q_{ij}(r+r_{ij})$ is usually small enough to neglect and the rest defined as follows: $r_{ij}$ is the interatomic distance between an atom of type $i$ and an atom of type $j$; $k_m$ is the largest $k$ value recorded in the experiment; $g(k)$ is the sharpening factor, which decreases with increasing $k$ and has the value of 1.0 at $k=0$ (it normally takes the form of $\sum_{\text{uc}}f_m/\sum_{\text{uc}}Z_m$) (where $Z_m=$ the atomic number, uc indicates unit composition); and $e^{-\alpha^2k^2}$ is the arbitrary convergence factor, (it usually takes the value such that $\alpha^2k_m^2=1.0$).

In terms of the pair functions, Eq. (7) presents the final form of the pair-distribution solution, where the right-hand side (rhs) is called $D(r)$ here:

$$D(r)=\sum_{\text{uc}}\sum_i\frac{N_{ij}}{r_{ij}}P_{ij}(r)$$

$$=2\pi^2r\rho_e\sum_{\text{uc}}Z_j+\int_0^{k_m}F(k)\sin(kr)dk , \tag{7}$$

where $N_{ij}$ is the average number of atoms in shell $i$ at a distance $r_{ij}$ from an atom of type $j$; $\rho_e=(N/V)\sum_{uc}/Z_j$ is the average electron density [$N$ is the number of unit compositions (uc) in the sample]; $F(k)=ki(k)e^{-\alpha^2k^2}$ is the reduced intensity function; and $i(k)=(I_{eu}/N-\sum_{uc}f_j^2)/g^2(k)$.

This method of pair functions is especially useful in cases where discrete intramolecular (chemical) distances exist in an amorphous solid which shows local chemical order and longer-range topological disorder. An excellent application was the study of Mozzi and Warren on $SiO_2$.[8] We do not take full advantage of this method in our modeling, however, because we do not calculate separate pair functions for all of our separate pairs of atoms. We, nonetheless, represent our transformed data as the function $D(r)$, which weighs the near-neighbor coordination properly.

### C. Computer calculation of models

In most structural modeling studies, physical ball-and-stick models have been used in which the directly recorded coordinates of the atoms were entered into the computer for structural computations. The diffraction intensity was then directly calculated using the Debye formula [Eq. (2)]. Manipulation of the models and reentering of the coordinates were repeated systematically until satisfactory results were reached. While this is not a widely used method for crystalline solids, it has advantages for a random aggregate of very small crystallites and for disordered materials. The computation is straightforward but rather time consuming. In this work, the computation was performed on a Honeywell 1130 computer, located at the University of Houston, as well as on a PDP 11-23 computer at the Exxon Corporate Research-Science Laboratories. The computing time was about four hours for a typical aggregate consisting of about 200 atoms, where the computation was carried out at a total of 110 values of the scattering wave vector.

Using this physical modeling approach, we have recently studied the structure of poorly crystalline (pc-) $MoS_2$.[9] In that case, since the basic layered structure is maintained, the modeling was aimed at studying essential crystalline parameters such as layer extent, the layer-stacking sequence, and the number of layers in a stack as well as the regularity (or disorder) in the layer stacking. We were able to obtain excellent agreement between experimental and calculated diffuse-intensity profiles of pc-$MoS_2$. In the case of amorphous $MoS_3$, the models have been constructed in a more complicated fashion. A large number of rotations were used to simulate the possible bending and twisting of the prismatic of atoms as shown in a later section. Extreme care was taken when the disordered chains were coupled, since an interchain distance of no less than 2.8 Å between the sulfur atoms had to be preserved to remain consistent with almost all transition-metal chalcogenides. It may perhaps appear somewhat arbitrary to calculate interference and radial distribution functions until the fit with experiment is deemed successful. However, these models are always rationalized and constrained by all known chemical and spectroscopic data and the fits, which are often rather hard to obtain, are treated as plausible rather than unique. Clearly, *not* to make such comparisons may limit severely the usefulness of a structural conjecture.

## IV. RESULTS OF DATA ANALYSIS

The earlier studies on $MoS_3$ suggested that this amorphous compound was not an independent compound but a mixture of $MoS_2$ and noncrystalline sulfur.[10–12] Later, from an analysis of the x-ray radial distribution functions, Diemann[13] concluded that $a$-$MoS_3$ was a genuine compound, although ambiguities remained concerning its detailed structure. Recently, a chainlike structure similar to that of the crystalline trichalcogenides of the neighboring IV*B* and V*B* elements was proposed by Liang and coworkers.[14] In this study, the dimerization of the metal atoms along the chain was inferred through radial distribution field (RDF) analysis of diffraction and EXAFS data, while XPS studies revealed the presence of a shorter disulfide bond, where the ratio of the number of shorter bonds to the normal sulfur bond was 1:2. More recent EXAFS (Ref. 15) results and magnetic measurements[16] are basically consistent with this structural model.

We will first examine here the nearest-neighbor coordinations of $a$-$MoS_3$ in more detail using the pair-function analysis. We will then compare the results of the computations on various models, in both $r$ space and $k$ space, with the experimental data. Finally, we will see that not only has the Fourier-transformed $r$-space pattern been fitted out to the fourth peak, but also the $k$-space pattern has been fitted throughout the region where the experimental data was collected. These two fits are complementary emphasizing the shorter-range (low-$r$-space) and longer-range (low-$k$-space) regimes.

### A. Profile of the diffraction pattern

It is interesting to inquire, as with pc-$MoS_2$,[9] if we are able to gather any information simply by looking at the profile of the diffraction pattern directly (Figs. 2 and 3). It consists of a prominent first peak at 1.0 $Å^{-1}$, a double peak at around 2.8 $Å^{-1}$, a shoulder immediately following the double peak at 4.0 $Å^{-1}$, and a broad peak at 5.5 $Å^{-1}$. It is quite common to have a sharp first peak for an amorphous material, although the precise origin of this prominent feature is often not well understood. The fact that the stacking of the sandwiched layers in pc-$MoS_2$ successfully produced a prominent peak at 1.0 $Å^{-1}$ (Ref. 9) suggests treating $a$-$MoS_3$ in a similar way. But the ensuing well-defined layer-related peak at 4.0 $Å^{-1}$ cannot then be made to disappear and the layered structure will therefore not be discussed further. However, a type of restricted planar (or quasiplanar) correlation will still be posited as the probable origin of the prominent first peak.

### B. Pair-function analysis

We now examine the $r$-space pattern, which is Fourier transformed from the reduced intensity. The reduced-intensity curve, $F(k)$, shown in Fig. 4 is obtained accord-

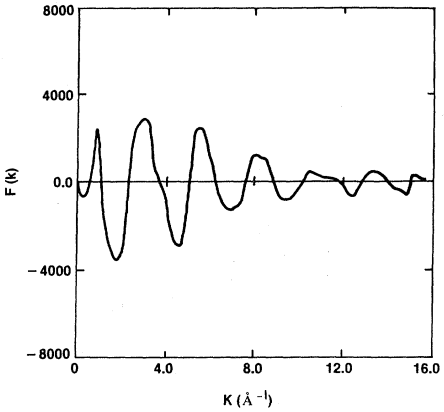


FIG. 4. The reduced intensity $F(k)$ of $a$-$MoS_3$, including a damping factor $\exp(-\alpha^2 k^2)$ to reduce the significance of the less accurate high-$k$ data.

ing to Eq. (3). Its Fourier transform $D(r)$ reveals a flat region and four peaks, located at 2.47, 2.90, 3.39, and 3.85 Å, in Fig. 5. Lying under the shoulder of the first peak, the second peak we believe to consist of mainly Mo-Mo pairs. The prominent first peak will be unmistakably assigned as a Mo-S peak. The Mo—S bond length 2.41 Å in crystalline $MoS_2$ is comparable to our value of 2.47 Å. However, we find that the Mo—S bond length can vary between about 2.45 and 2.60 Å as found in many coordination crystals containing Mo and S atoms,[17] which gives a possible explanation for the broadening of the first peak [full width at half maximum (FWHM)=0.15 Å, Table I]. The estimation of the area of the first peak, shown in Table I, suggests about six sulfur atoms around each molybdenum atom. The third and the fourth peaks could be partly generated by Mo-Mo pairs, where the source of broadening of the peaks is at present unclear. The missing indication of the disulfide bond at 2.05 Å is thought to be caused by the cancellation between the ripples of the first peak and the weak contribution due to the small scattering factor of the sulfur atoms. The continuous increasing background in the region beyond 4.2 Å indicates significant disorder. Therefore, it would be unrealistic to discuss that region without building a larger model.

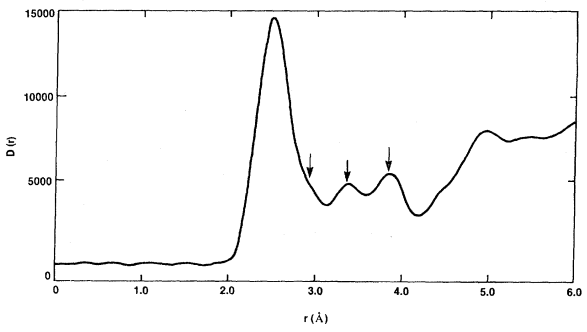


FIG. 5. The experimental radial pair-distribution function $D(r)$ for $a$-$MoS_3$. The arrows indicate prominent interatomic distances whose contributions must be rationalized. Beyond the first four, oscillations are considered due to combinations of distances of different interatomic pairs.

TABLE I. Nearest-neighbor (NN) atoms estimated with Gaussian distribution.

| Peak | Position (Å) | Assumed pair | Number of NN atoms for Mo | $\sigma$ (Å) |
|---|---|---|---|---|
| 1 | 2.47 | Mo-S | 6.83 | 0.15 |
| 2 | 2.90 | Mo-Mo | 1.48 | 0.09 |
| 3 | 3.39 | Mo-Mo | 2.48 | 0.16 |
| 4 | 3.85 | Mo-Mo | 2.63 | 0.10 |

### C. Model calculation

Before going into the details of the computations of the chainlike model, we should note that a three-dimensionally (3D) coordinated random network model involving sixfold-coordinated Mo and twofold-coordinated S is not possible in this material, because it would require the number of next nearest Mo-Mo neighbor atoms to be six. That would imply that the second, third, and fourth peaks of the RDF were all due to this Mo-Mo shell.

The computations for each model have first been carried out in $k$ space using Eq. (2) after which $r$ space values are obtained by Fourier transforming the $k$ space results as in Eq. (7). In order to avoid ambiguities arising from the treatment of the data, such as truncation effects, the analysis parameters including integration region, sharpening factor, convergence factor, etc., have been applied to both the experimental reduced intensity and the calculated intensities in an identical fashion. The S atoms to form the disulfide bonds are specially distinguished and labeled in this study. While they do not contribute markedly to the derived pair function, the disulfide bonds must be treated with great care to ensure a physically reasonable structure.

#### *1. Basic chain structure*

The basic chain structure is constructed based on the previous work by Liang *et al.*[14] except that the disulfide species are placed between the Mo dimers to be consistent with most known Mo-S coordination structures.[17] Different bond lengths of Mo-S pairs have been assigned in the model calculations in order to simulate the first peak at 2.47 Å in $r$ space. The normal Mo—S bond is assigned to be 2.40 Å, where the distinguished ones are at 2.60 Å. Each molybdenum atom is surrounded by six sulfur atoms. Along the chain, a bond length of 2.8 Å is assigned to the Mo dimer while the normal Mo-Mo distance is 3.4 Å. The two different Mo-Mo distances (2.8 and 3.4 Å) are arranged alternately along the chain where three sulfur atoms form a plane bisecting every Mo-Mo pair. In this way, a prismatic configuration has been arranged about each molybdenum atom and six surrounding sulfur atoms as shown in Fig. 6. The disulfide bonds are initially introduced into every other sulfur plane.

The $k$-space patterns of a straight-chain model with various numbers of molybdenum atoms along the chain are shown in Fig. 7. The sharpening of the peak at 4.1 $Å^{-1}$ is caused by the increasing of the length of the chain. The large background in the small-$k$ region ($k < 1.0$ $Å^{-1}$)

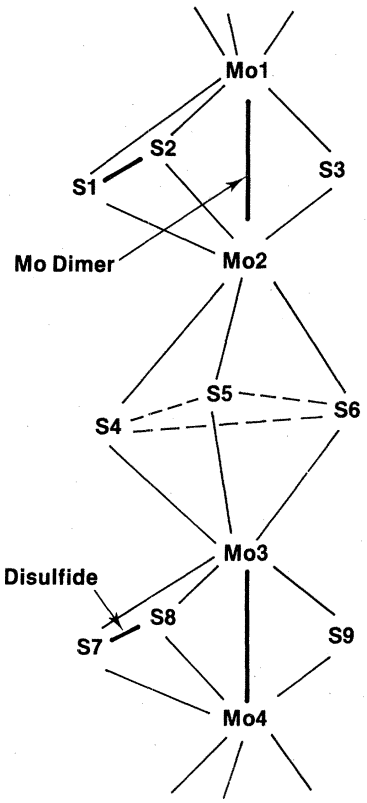


FIG. 6. The single-chain model for computation. The interatomic distances of the model are given in Table III.

is understood simply to be the shape transform factor for a small rotated molecule. For an increasingly bended chain with variable bending, the peak at 4.1 $\text{Å}^{-1}$ weakens and broadens as shown in curve C in Fig. 7. Although not

TABLE II. The interatomic distances of the chain structure shown in Fig. 6.

| Atoms | Distance (Å) |
|---|---|
| Mo(1)-Mo(2) | 2.80 |
| Mo(2)-Mo(3) | 3.40 |
| Mo(3)-Mo(4) | 2.80 |
| Mo(1)-S(1) | 2.60 |
| Mo(1)-S(2) | 2.60 |
| Mo(1)-S(3) | 2.40 |
| Mo(2)-S(1) | 2.60 |
| Mo(2)-S(2) | 2.60 |
| Mo(2)-S(3) | 2.40 |
| Mo(2)-S(4) | 2.40 |
| Mo(2)-S(5) | 2.40 |
| Mo(3)-S(4) | 2.40 |
| Mo(3)-S(5) | 2.40 |
| Mo(3)-S(6) | 2.40 |
| S(1)-S(2) | 2.05 |
| S(1)-S(3) | 3.52 |
| S(2)-S(3) | 3.52 |
| S(4)-S(5) | 3.38 |
| S(4)-S(6) | 3.38 |
| S(5)-S(6) | 3.38 |

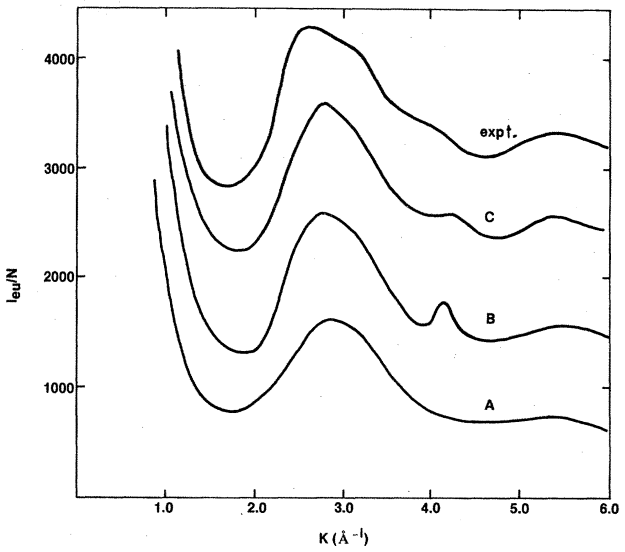


FIG. 7. Calculated intensity for a single-chain model. *A*, straight chain with two Mo atoms along the chain. *B*, straight chain with eight Mo atoms. *C*, arbitrarily bent chain with eight Mo atoms and a bend angle of 12° between short and long Mo pairs.

shown in the figure, we note that varying the distance of the normal Mo—Mo bond moves the shoulder around 3.1 $\text{Å}^{-1}$, while the rest of the pattern is not affected very much. When we compare the full reduced intensity of the model of a bent chain to the experimental one, the resemblance between the two as shown in Fig. 8 is clear. The first peak in the upper curve, near $k \sim 0.5$, is simply a result of multiplication of the high background at low $k$ by $k$, which varies from 0.0 to 15.0 $\text{Å}^{-1}$ while the actual data peak at $k = 1$ $\text{Å}^{-1}$ remains to be explained. In Fig. 9, however, the *r*-space comparison clearly requires some coupling of the basic chains in order to account for the data; as noted earlier, both *k*- and *r*-space agreements are essential.

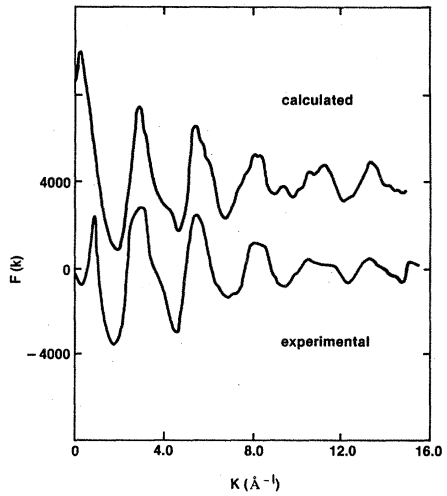


FIG. 8. Calculated intensity of an arbitrary bended (12°) single-chain model compared to the experimental data.

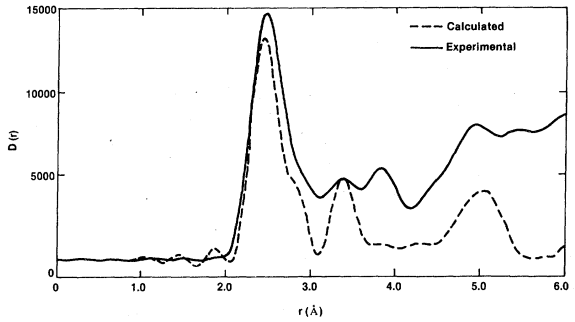


FIG. 9. Radial pair-distribution function $D(r)$ of an arbitrarily bended (12°) single-chain model compared to experiment.

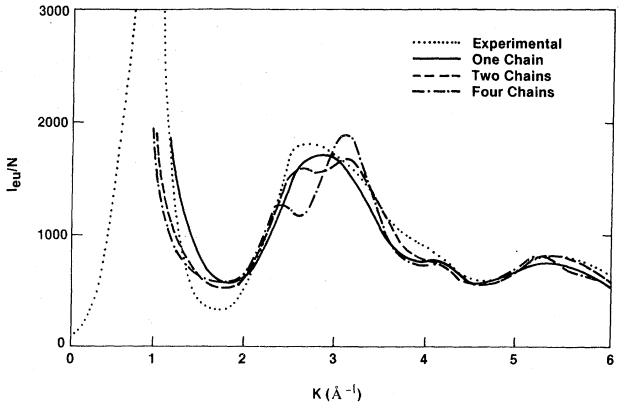


FIG. 11. The calculated intensities of coupled chains of four Mo atoms of models (a) and (b) of Fig. 10.

### 2. *Microcrystalline $MX_3$ model*

As stated previously, the structural model employed in our RDF analysis is mainly based on the crystalline trichalcogenides of groups VI*B* and V*B*.[14] In these crystalline compounds, the structures exhibit extensive interchain coupling where the coupled chains may form a pseudolayered structure.[3] We therefore investigate models based on these structures. Schematics of the models studied are shown in Fig. 10 with the calculated intensity patterns shown in Fig. 11 for straight chains with four Mo atoms per chain.

The calculated diffraction patterns of coupled chains are compared in Fig. 11 with the single chain and with experiment. In the case of two coupled chains [Fig. 10(a)], the results reveal a double peak at about 2.8 Å$^{-1}$, a small peak at 4.1 Å$^{-1}$ immediately following the double peak, and a peak at 5.4 Å$^{-1}$ in a way suggestive of the experimental data. The 3.2-Å$^{-1}$ peak develops only through the coupling of two chains. When two more chains are added [Fig. 10(b)], however, the diffuse structure is too enhanced both at 3.2 and 5.3 Å$^{-1}$. We therefore conclude that the interchain correlation cannot go beyond two chains.

Finally, we also investigated several versions of the crystalline $MX_3$ model to include coupled chains as a pseudolayer and a van der Waals gap between the layers.[3] One of these examples are shown in Fig. 10(c). A low angle peak $\sim 1$ Å$^{-1}$ is generated in this case through the interferences associated with the distance $d$ of the model. But the sharp structures of the interference function cannot be successfully removed without severe bending or distortion to a degree that the order can no longer be considered as microcrystal. We therefore conclude that a microcrystalline version of $MX_3$ is not satisfactory.

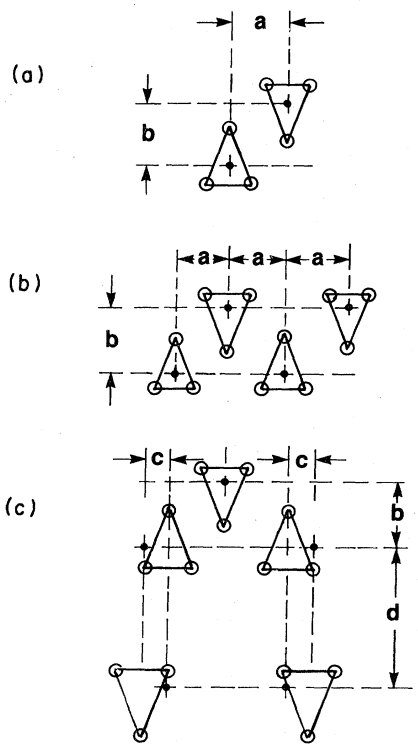


FIG. 10. Schematics of the structural models involving coupled chains as in the crystalline trichalcogenides.

### 3. *Ribbonlike model*

Through the modeling work discussed so far, we realize that the order along the chain should not be extended beyond four Mo atoms and the correlation between the chains should not go beyond two chains in order to eliminate sharp features of the calculated patterns. Our goal now is to construct a model structure with these requirements in disorder and yet to produce the satisfactory fits in both $k$-space and $r$-space experimental data.

Our calculation starts with a basic model with two chains coupled together. However, with the disulfide bond at the location shown in Fig. 6, we find that it is difficult to fit the $k$-space pattern and construct a physically reasonable model at the same time. By this we mean that joint requirement of bending and coupling cannot be met. We note, however, that the disulfide bonds may be located sideways as in the molecular structure of anions such as $[Mo_4(NO)_4S_3(S_2)_5]^{4-}$.[18] Therefore, a new model is constructed as shown in Fig. 12.

In this new model, with the disulfide bond formed by two sulfur atoms between two separate triangular sulfur planes, we are able to provide room for the coupling of the chains. This essential coupling is made possible only because some of the sulfur atoms are shared by the molybde-

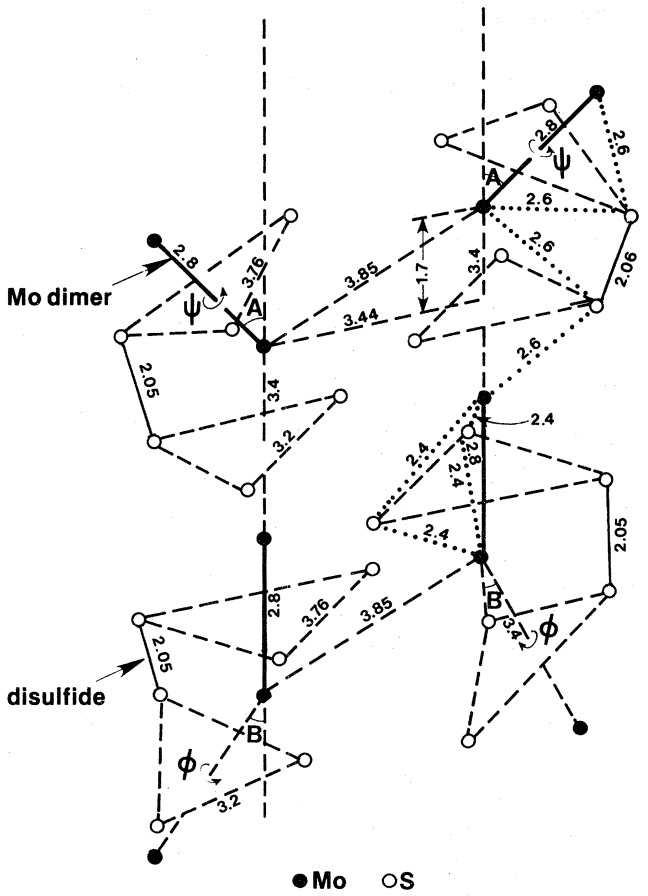


FIG. 12. A model of two coupled chains. The coordinates of the atoms are given in Table IV.

num atoms of the neighboring chain, as in the case of the chainlike transition-metal trichalcogenides.[3] The length of this type of Mo—S bond is assigned to be about 2.6 Å. The interchain molybdenum distances are now about 3.85 Å. In order to keep interchain S-S distances within a reasonable range (greater than 2.8 Å), it is necessary to have two chains separate after coupling for about 6 Å; in other words, the coupling of the chains will be *turned on and off constantly* as the model extends, while chains curve through the space. It is quite clear that two coupled chains, without bending or spreading, would generate, as noted earlier, excessively sharp structure and too large a fourth peak in the $r$-space pattern. In addition, the model may be extended with more freedom simply through the sharing of the corner molybdenum atoms of the structure shown in Fig. 12.

Before we discuss various $k$-space calculations, the radial pair distribution of the model may be examined to see if enough pairs for the first four peaks can be generated, as we only deal with the relatively small model of Fig. 12 in our $k$-space calculations. The radial pair distributions of this model, collected through a Fourier transformation of the calculated $k$-space data, can only provide us with a general view on that account. Therefore, the radial pair distribution $D(r)$ along a *single* chain of extended length (eight Mo atoms) is calculated and shown in Fig. 13 (curve $A$), while curve $B$ in Fig. 13 shows the $D(r)$ contributed by

TABLE III. The coordinates of the atoms of the proposed model shown in Fig. 12. $I$ goes from top to bottom of the left chain, then the right chain.

| | $X(I)$ | $Y(I)$ | $Z(I)$ |
|---|---|---|---|
| 1 | 0.000 | 0 | 0 |
| 2 | −0.418 | −0.579 | −2.500 |
| 3 | 1.694 | −1.684 | −0.237 |
| 4 | 1.019 | 1.949 | −0.950 |
| 5 | 2.047 | 0 | −1.910 |
| 6 | 0.338 | 0.973 | −3.610 |
| 7 | 1.732 | −1.665 | −3.610 |
| 8 | 3.322 | 1.116 | −3.610 |
| 9 | 2.047 | 0 | −5.310 |
| 10 | 0.143 | 1.084 | −6.710 |
| 11 | 1.552 | −1.885 | −6.710 |
| 12 | 3.420 | 1.384 | −6.710 |
| 13 | 2.047 | 0 | −8.110 |
| 14 | −0.531 | 0.160 | −8.486 |
| 15 | 1.432 | −1.642 | −9.749 |
| 16 | 1.651 | 1.590 | −9.899 |
| 17 | 7.538 | 0 | 1.700 |
| 18 | 7.955 | 0.580 | −0.800 |
| 19 | 5.842 | 1.581 | 1.463 |
| 20 | 6.522 | −1.951 | 0.740 |
| 21 | 5.491 | −0.063 | −0.210 |
| 22 | 7.302 | −0.974 | −1.910 |
| 23 | 5.803 | 1.122 | −1.910 |
| 24 | 4.219 | −1.122 | −1.910 |
| 25 | 5.491 | −1.093 | −5.010 |
| 26 | 7.397 | −1.084 | −5.010 |
| 27 | 5.983 | 1.883 | −9.010 |
| 28 | 4.120 | −1.389 | −5.010 |
| 29 | 5.491 | −0.003 | −6.410 |
| 30 | 8.070 | −0.159 | −6.708 |
| 31 | 6.104 | 1.640 | −8.049 |
| 32 | 5.839 | −1.553 | −8.199 |

*interchain* pairs, in which only pairs of short distances are included. The estimations of the nearest-neighbor atoms of the calculated model are compared with the corresponding expectation values in Table IV. While curve $C$, the combination of curves $A$ and $B$, in Fig. 13 shows fairly good agreement with the experimental data (curve $D$), the calculated peaks are too sharp because only discrete values

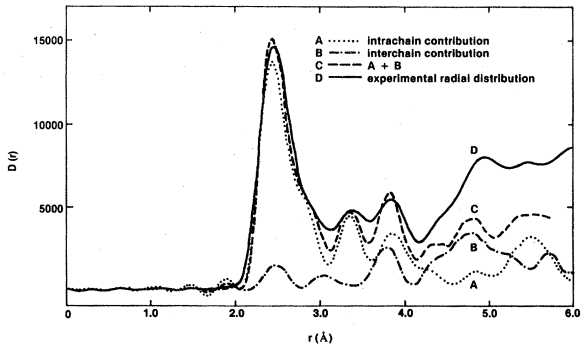


FIG. 13. The calculated $r$-space pattern from a pair of chains shown in Fig. 12 compared to the experimental one.

TABLE IV. Nearest-neighbor (NN) atoms calculated compared with the expected value of the model.

| Peak | Position (Å) | Pair | Number of NN atoms for Mo (expected)[a] | Curve A in Fig. 17 (calculated) |
|---|---|---|---|---|
| 1 | 2.40–2.60 | Mo-S | 6.5 | 6.31 |
| 2 | 2.80 | Mo-Mo | 1.0 | 1.0 |
| 3 | 3.39 | Mo-Mo | 1.0 | 0.94 |
| 4 | 3.85 | Mo-Mo | 1.25 | 1.25 |

[a]Other contributions, such as Mo-S, S-S, in peaks 2, 3, and 4 were excluded.

have been assigned to the corresponding pairs of the model rather than the assumed variable values. Nevertheless, our task now is to see if the $k$-space calculations will provide an adequate agreement as well.

The reduced intensity for the coupled chains in Fig. 12 with four molybdenum atoms along the chain is compared with experiment in Fig. 14. Similar to the reduced intensity of the previous calculated single-chain model, the new $k$-space data reveal the general features of the experimental curve. The main differences are the presence of the broad double peak and the clean valley which follows it. Extension of these coupled chains beyond four Mo atoms yields essentially similar patterns.

With no prominent first peak in evidence and the shoulder at 4.0 $Å^{-1}$ not properly revealed, we believe that an imposed planar correlation is required. This planar correlation arises naturally if we accept the coupled pairs and require only that, as they fold and turn, they fill space. To include them, we simply stack two pairs of four-atom molybdenum chains on top of each other with an estimated van der Waals gap of 6.30 Å betwen the Mo atoms of the pairs of chains. The reasoning behind this is that the stacking will not get in the way when we connect the pairs of the chains by the corners, as required by an amorhpous model. The stacking of the pairs of the chains

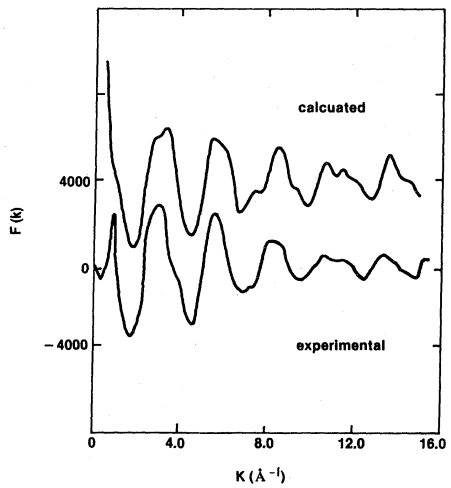


FIG. 14. The reduced intensity of a pair of chains shown in Fig. 12 is compared to the experimental one.

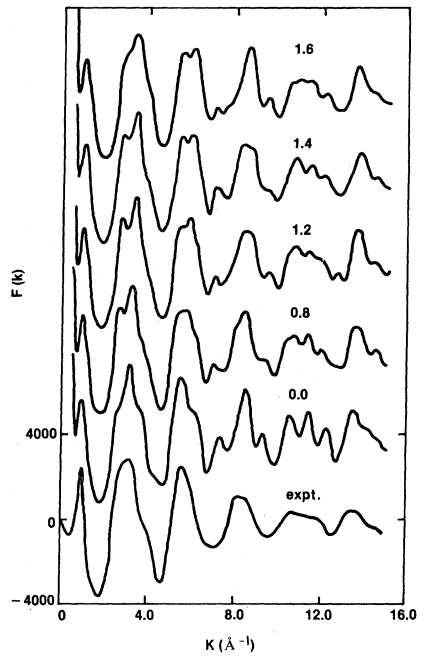


FIG. 15. The $k$-space patterns of two pairs of chains stacked with different planar rotations about an axis normal to the chain pair.

immediately produces the prominent first peak at 1.0 $Å^{-1}$ due to the planar correlations of molybdenum ribbonlike planes at a distance of 6.30 Å, as shown in Fig. 15. Various calculations for the stacking with different in-plane rotations are included. The double peak at 2.8 $Å^{-1}$ is relatively separated in most cases. Surprisingly, most patterns show a well-shaped shoulder at around 4.0 $Å^{-1}$.

In comparing these calculations to the experimental pattern, we now begin to achieve an adequate agreement in $k$ space. This is best illustrated in Fig. 16, where a pattern for the in-plane rotation of 1.4 rad between pairs of

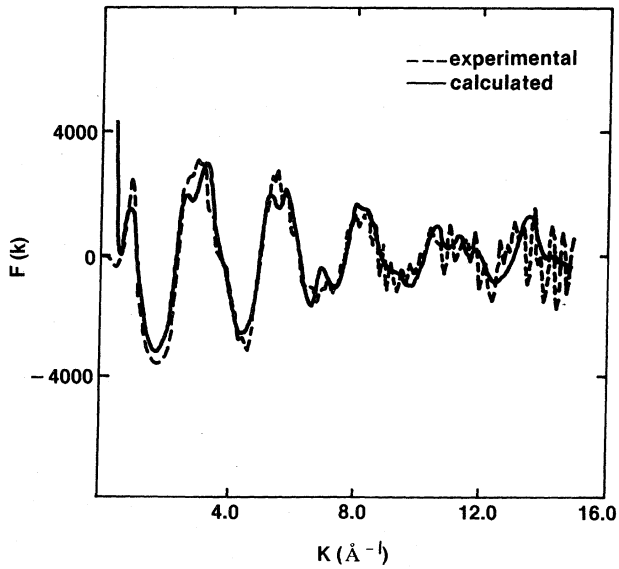


FIG. 16. The reduced intensity of a stacked-pair model with 1.4 rad of rotation is compared to the experimental one.

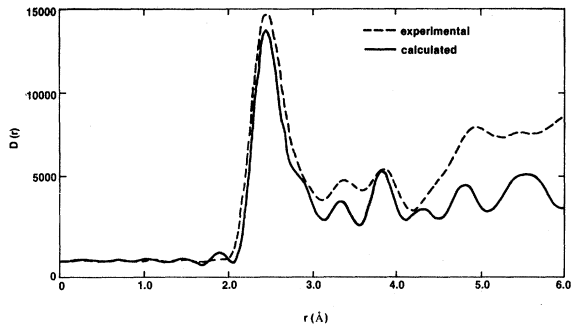


FIG. 17. The comparison between the experimental $r$-space pattern and that of a stacked pair of coupled chains with 1.4 rad of rotation.

ribbons is compared to the experimental pattern, which here is unsmoothed. Discrepancies still exist. But, with a model of this size, a quantitative perfect fit is not manageable because of the large molecular disorders involved in the amorphous material and the difficulty of incorporating the full range of this disorder. Figure 17 shows the comparison between the calculated pattern (1.4-rad rotation of stacked ribbons) and the experimental one in $r$ space. The calculated pattern falls short, as expected, on some aspect as far as the area is concerned, but the demonstration shows nonetheless the essential ingredients of the "real" structure. Actually, the calculated $r$-space pattern would take the form of curve C in Fig. 13 with the extension of the chainlike network.

## V. SUMMARY AND CONCLUSIONS

In this study of the structure of $a$-$MoS_3$, we have employed a consistent $r$-space and $k$-space fitting process in which small $r$ corresponds to large $k$ and vice versa. Eventually we were able to reach a rather satisfactory result which is consistent with not only the local order obtained previously from RDF,[14] XPS,[14] EXAFS,[15] and magnetic measurements[16] but also the intermediate-range structural correlations observed as prominent features in the low-angle region of the x-ray diffraction pattern. However, the postulated sideways location of the disulfide bond may seem somewhat surprising. The domination of the crossover of the pairs of the chains had not been previously anticipated.[14] An important finding is that the prominent first peak in $k$ space may be generated by a narrow (ribbonlike) planar correlation, made possible through a suitable stacking of the chain pairs of the model. During the process of investigation, quite often a one-sided (i.e., an agreement either in $k$ space or in $r$ space) result has been obtained. Since an exact fitting is out of the question, the one-sided fitting soon proved to be unsatisfactory in other respects. To fit both $k$-space and $r$-space patterns reasonably well with a physically sound model provides us, we believe, with substantial structural information on this material. To that extent we believe that both our process and results on $a$-$MoS_3$ have been successful.

## ACKNOWLEDGMENTS

We wish to thank Dr. A. J. Jacobson and Dr. I. E. Stiefel for many helpful discussions. The work at Standord Synchrotron Radiation Laboratory was supported by the U.S. Department of Energy under Contract No. DE-AC02-82RR-1300.

*Present address: Physics Department, Tamkang University, Taipei, Taiwan, Republic of China.

[1]See, for example, *Topical Conference on Atomic Scale Structure of Amorphous Solids, Yorktown Heights, 1978,* edited by G. S. Cargill III and P. Chaudhari (North-Holland, New York, 1979).

[2]For examples of successful modeling, see J. Bell and P. Dean, Philos. Mag. 25, 1381 (1972) for $SiO_2$; G. S. Cargill, in *Solid State Physics,* edited by F. Seitz and D. Turnbull (Academic, New York, 1975), p. 227, for metallic glasses; P. Steinhardt, R. Alben, and D. Weaire, J. Non-Cryst. Solids 15, 199 (1974) for amorphous Ge.

[3]See, for example, the series of *Physics and Chemistry of Materials with Layered Structures: Intercalation Compounds,* edited by F. Levy (Reidel, Holland, 1979); for crystal structures of dichalcogenides and trichalcogenides, see Vol. 5 of the series by F. Hulliger.

[4]A. J. Jacobson, R. R. Chianelli, S. M. Rich, and M. S. Whittingham, Mater. Res. Bull. 14, 1437 (1979).

[5]K. S. Liang (unpublished).

[6]B. E. Warren, *X-Ray Diffraction* (Addison-Wesley, Reading, Mass., 1964).

[7]*International Tables for X-Ray Crystallography,* edited by N. F. M. Henry and K. Lonsdale (Kynoch, Birmingham, 1952), Vol. III.

[8]R. L. Mozzi and B. E. Warren, J. Appl. Crystallgr. 2, 164 (1969).

[9]F. Z. Chien, S. C. Moss, K. S. Liang, and R. R. Chianelli, J. Phys. (Paris) Colloq. 40, C4-273 (1981).

[10]R. J. H. Voorhoeve and H. M. B. Wolters, Z. Anorg. Allg. Chem. 376, 165 (1970).

[11]P. Ratnasamy, L. Rodrique, and A. J. Leonard, J. Phys. Chem. 77, 3242 (1973).

[12]G. C. Stevens and T. Edmonds, J. Catal. 37, 544 (1975).

[13]E. Diemann, Z. Anorg. Allg. Chem. 432, 127 (1977).

[14]K. S. Liang, J. P. de Neufville, A. J. Jacobson, R. R. Chianelli, and F. Betts, J. Non-Cryst. Solids 35 and 36, 1249 (1980); K. S. Liang, S. P. Cramer, D. C. Johnston, C. H. Chang, A. J. Jacobson, J. P. de Neufville, and R. R. Chianelli, *ibid.* 42, 345 (1980).

[15]S. P. Cramer, K. S. Liang, A. J. Jacobson, C. H. Chang, and R. R. Chianelli, J. Am. Chem. Soc. (to be published).

[16]D. C. Johnston, private communication.

[17]E. I. Stiefel, in *Molybdenum and Molybdenum Containing Enzymes,* edited by M. P. Coughlan (Pergamon, New York, 1980), Chap. 2.

[18]A. Muller, W. Eitzner, and N. Mohan, Angew. Chem. 18, 168 (1979).